

# HYSTERESIS AND VIBRATION COMPENSATION IN PIEZOELECTRIC ACTUATORS BY INTEGRATING CHARGE CONTROL AND INVERSE FEEDFORWARD<sup>1</sup>

G M Clayton<sup>\*,2</sup> S Tien<sup>\*</sup> A J Fleming<sup>\*\*,3</sup>  
S O R Moheimani<sup>\*\*</sup> S Devasia<sup>\*</sup>

*\* Department of Mechanical Engineering  
University of Washington  
Box 352600, Seattle, WA 98195, USA*

*\*\* School of Electrical Engineering and Computer Science  
University of Newcastle  
University Drive, Callaghan, NSW 2308, Australia*

Abstract: In this paper we address the problems of hysteresis and vibrations that limit the accuracy of piezoelectric positioners. It is widely known that the use of charge control significantly reduces hysteresis, thus enabling high-accuracy positioning during low speed operations. However, charge control is unable to reduce vibrations that limit the positioning bandwidth. Our main contribution is to overcome this bandwidth limitation by augmenting charge control with inverse feedforward to compensate for vibrations, resulting in a high-bandwidth, high-accuracy positioning system. We apply this integrated method to a piezoelectric tube actuator and experimental results are presented to illustrate the positioning improvements with the proposed integrated approach.

Keywords: Hysteresis, Vibration, Piezopositioners, Feedforward, Charge Control

## 1. INTRODUCTION

In this article we address the problems of hysteresis and induced mechanical vibrations that limit the accuracy of piezoelectric positioners (piezopositioners). Piezopositioners offer sub-angstrom positioning resolution over micron scale ranges and have been widely used in mechatronic systems developed for such purposes as nanofabrication (Quate, 1997) and scanning probe microscopy (SPM) (Binnig and Smith, 1986). Although the positioning resolution of piezopositioners is high,

the positioning accuracy is severely limited by hysteresis and vibrations. This loss of positioning accuracy can lead to undesired effects such as errant surface modification in nanofabrication (Hiura, 2003) or image distortions in scanning probe microscopy (Barrett and Quate, 1991). In this article we propose an integrated approach to compensate for both effects. Recent improvements in charge amplifiers have enabled easy implementation of charge control (Fleming and Moheimani, 2006) (where the piezo is driven by charge as opposed to voltage), which significantly reduces hysteresis-caused positioning errors (Newcomb and Flinn, 1982). However, charge control cannot reduce vibration-caused positioning

---

<sup>1</sup> This work supported by NSF Grant: CMS 0301787

<sup>2</sup> email: gclayton@u.washington.edu

<sup>3</sup> email: andrew.fleming@newcastle.edu.au

errors that limit the effective bandwidth (operation speed) of the piezopositioner. Our main contribution is to overcome this bandwidth limitation by augmenting charge control with inverse feedforward to compensate for vibrations (Bayo, 1987), achieving reduction in both hysteresis- and vibration-caused error. We apply this integrated method to a piezoelectric tube actuator and experimental results are presented.

### 1.1 Reducing hysteresis-caused positioning error

In piezopositioners, the hysteresis nonlinearity causes a *looping* behavior between the input voltage and the output displacement (Cao and Evans, 1993). The amount of hysteresis error tends to decrease with operating range, so a typical hysteresis reduction strategy is to operate the piezopositioner at a small fraction of its maximum range (e.g., nanometers as opposed to microns). This method, although effective at reducing the magnitude of the hysteresis error, not only limits the piezopositioner's ability to position over large ranges, but also does not reduce the percentage error with respect to the smaller operating range.

Feedback methods have been widely used to reduce hysteresis-caused positioning error in piezopositioners. Many feedback controllers have been implemented including proportional integral derivative (PID) (Kouno, 1982) and state feedback (Okazaki, 1990). The advantages of feedback control include ease of implementation and robustness to modeling error, but the effectiveness of these methods is limited to low frequency operations due to excessive transient error at high frequencies. Generally, to improve controller performance, feedback gains can be increased, however, typical piezopositioners have low damping, and thus a low gain margin, meaning that high gain control causes instability. Therefore, feedback methods can reduce hysteresis-caused positioning errors at low frequencies, but fail to substantially improve precision as the operating frequency is increased.

Feedforward techniques can be used to provide hysteresis compensation by inverting mathematical models of the hysteresis nonlinearity to determine hysteresis canceling inputs. Many methods have been implemented based on different hysteresis models including the Preisach model (Ge and Jouaneh, 1996) and the Prandtl-Ishlinskii model (Kuhnene and Janocha, 2001). Although inverse feedforward is effective, reducing hysteresis by 80-90%, modeling of the nonlinear hysteretic behavior of the system can be difficult depending on the complexity (order) of the model being used. It is noted that high-order hysteresis models are needed to capture the nonlinearity accurately over

a wide range of operating conditions. Therefore, inverse feedforward techniques can effectively reduce hysteresis error (even at high frequencies), but modeling and inverting the nonlinearity may be computationally prohibitive.

The frequency limitations of feedback control and the computational difficulties of feedforward control can be avoided by using charge control (Newcomb and Flinn, 1982). The hysteresis nonlinearity in piezopositioners occurs between the voltage input and the induced charge, thus, by controlling charge directly, hysteresis can be reduced by up to 90% (Fleming and Moheimani, 2006). Historically, implementation difficulties have limited the use of direct charge control (Kaizuka and Siu, 1988), however, recent improvements in charge amplifiers have allowed for the straightforward implementation of charge control (Fleming and Moheimani, 2006), enabling wide-band, computation-free hysteresis reduction.

### 1.2 Reducing vibration-caused error

Induced mechanical vibrations occur in piezopositioners when the input excites the dynamic response of the positioner. Specifically, vibrations tend to degrade positioning accuracy as the main frequency content of the input becomes close to the first resonance frequency of the system and become significant at approximately  $1/10^{th}$  of this frequency (Barrett and Quate, 1991). A simple approach to reduce vibration-induced error is to choose system inputs that avoid exciting the piezopositioner's vibrational dynamics. Specifically, vibrations can be decreased by limiting the input frequency content to well below the system resonance (low speed operation). Alternatively, to allow for higher speed operation, the first resonance frequency of the system can be increased by optimizing the geometry of the piezopositioner. This optimization, however, usually results in a smaller piezopositioner, limiting the piezopositioner's maximum range. Therefore, by redesigning aspects of the system we either limit the range or the operational frequency of the piezopositioner.

Feedback control techniques similar to those used to reduce hysteresis can be applied directly to reduce vibrations as well, but they suffer the same low frequency-range limitations. In contrast, inverse feedforward methods can reduce vibration effects over a broad range of frequencies. In inverse feedforward control a mathematical model of the system's linear vibrational dynamics is developed and used to determine vibration compensating inputs. Inverse feedforward has been shown to significantly reduce vibrations in piezopositioners using a variety of schemes such as full system in-

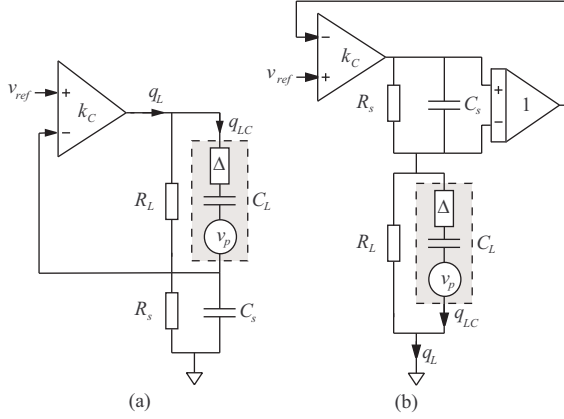


Fig. 1. Simplified circuit diagrams for (a) a typical charge amplifier and (b) a DC accurate grounded-load charge amplifier.

version (Croft and Devasia, 1998), optimal inversion (Croft and Devasia, 1999), and robust inversion (Schitter and Stemmer, 2003), but these techniques only invert the linear dynamics of the system and ignore the hysteresis nonlinearity. Thus, the accuracy of the system model is limited, which in turn limits the positioning accuracy. Therefore, linear inverse feedforward techniques work well to reduce vibration-caused positioning errors in linear systems, but cannot improve positioning error associated with nonlinearities such as hysteresis.

### 1.3 The integrated approach

In this article we present an integrated approach using charge control and inverse feedforward to compensate for hysteresis and vibrations in piezopositioners. It is noted that charge control can reduce hysteresis, but cannot reduce vibration effects. On the other hand, linear inverse feedforward can reduce vibration effects, but cannot reduce the nonlinear hysteresis effects. Therefore, we propose to first linearize the input-output hysteresis using charge control, and then, second, invert this linearized system to find vibration canceling inputs. Thus, the proposed integrated approach offers wide band hysteresis and vibration compensation while remaining relatively easy to implement. The remainder of this article is organized as follows. Background information is presented in section 2. The experimental setup and results are discussed in section 3. Finally, in section 4, concluding remarks are presented.

## 2. BACKGROUND

### 2.1 Charge Control

Operating piezopositioners with charge control, as opposed to voltage control, has been shown to

significantly reduce the effects of hysteresis (Newcomb and Flinn, 1982), however implementation issues have limited its widespread use.

#### 2.1.1. Difficulties associated with charge control

A circuit diagram for a typically used charge amplifier is shown in Figure 1(a) with the piezoelectric load shown in gray. The high gain feedback amplifier ( $k_C$ ) works to equate the applied reference voltage ( $v_{ref}$ ), to the voltage across a sensing capacitor ( $C_s$ ). By neglecting the resistances  $R_L$  and  $R_s$  the load charge ( $q_L$ ) for frequencies within the bandwidth of the control loop is given by

$$\frac{q_L}{v_{ref}} = C_s. \quad (1)$$

Thus we have a charge amplifier with gain  $C_s$  *Columbs/Volt*.

This charge amplifier has two primary drawbacks. First, both piezopositioner leads are floating with respect to ground, which creates difficulties because it is typical in practice to ground one of these leads. Second, due to the resistances  $R_L$  and  $R_s$  that model the parasitic leakage from the input terminals of the feedback opamps and capacitor dielectric leakage, low frequency performance is limited. For example, consider only the resistance  $R_L$ . The actual charge  $q_{LC}(s)$  flowing through the load transducer contains a high-pass filter with cutoff  $\omega_c = \frac{1}{R_L C_L}$ . That is,

$$\frac{q_{LC}(s)}{v_{ref}(s)} = C_s \frac{s}{s + \frac{1}{R_L C_L}}. \quad (2)$$

Such low-frequency performance precludes the use of charge amplifiers in applications requiring accurate low-frequency tracking.

#### 2.1.2. DC accurate grounded-load charge amplifier

The two drawbacks with typical charge amplifiers have recently been overcome with the development of a new class of DC-accurate grounded-load charge amplifiers (Fleming and Moheimani, 2006), shown in Figure 1(b). As seen in the Figure, this new amplifier is capable of driving grounded loads, and can thus be applied to typical piezopositioner systems. To provide improved low frequency performance, the resistances  $R_L$  and  $R_s$  can be chosen to eliminate the high pass filter in Equation 2 (Yi and Veillette, 2005). The transfer function from the reference voltage ( $v_{ref}$ ) to the load charge ( $q_L$ ) can be found by first finding the transfer function between the input voltage and the total charge ( $q_L$ ) on the load impedance,

$$\frac{q_L(s)}{v_{ref}(s)} = C_s \frac{s + \frac{1}{C_s R_s}}{s}, \quad (3)$$

and then combining it with the actual charge flowing through the load transducer from Equations 1 and 2, yielding

$$\frac{q_{LC}(s)}{v_{ref}(s)} = C_s \frac{s + \frac{1}{C_s R_s}}{s} \frac{s}{s + \frac{1}{R_L C_L}}. \quad (4)$$

Thus, by choosing  $C_L R_L = C_s R_s$ , we have

$$\frac{q_{LC}(s)}{v_{ref}(s)} = C_s, \quad (5)$$

which is an amplifier with no low-frequency dynamics and a constant gain ( $C_s$ ) *Columbs/Volt*. Effectively the voltage amplifier, comprised of the two resistances  $R_L$  and  $R_s$ , mimics an ideal charge amplifier at low frequencies.

## 2.2 Inverse Feedforward

To compensate for induced mechanical vibrations in the proposed integrated approach, inverse feedforward control is used. In the exact inverse feedforward scheme (Bayo, 1987), the system's linear vibrational dynamics ( $G(s)$ ) are modeled and inverted, resulting in the inverse system dynamics ( $G^{-1}(s)$ ). To determine a vibration compensating input ( $u_{ff}$ ) the desired trajectory ( $y_d$ ) is passed through the inverse dynamics as

$$u_{ff} = G^{-1}y_d. \quad (6)$$

This input can then be applied to the system, yielding the output as desired. While this approach allows for exact tracking of the desired trajectory, the inputs may be excessively large, causing actuator saturation. Furthermore, if modeling errors occur the desired trajectory cannot be perfectly tracked.

**2.2.1. Optimal inverse feedforward method** In this article an optimal inverse feedforward method is used (Dewey et al., 1998). By using an optimal method, tracking performance can be sacrificed for lower input magnitudes through minimization of the following cost function:

$$J(u) = \int_{-\infty}^{\infty} \{u^*(j\omega)R(j\omega)u(j\omega) + [y(j\omega) - y_d(j\omega)]^*Q(j\omega)[y(j\omega) - y_d(j\omega)]\}, \quad (7)$$

where all terms are expressed in the frequency domain,  $u$  is the input,  $y$  is the output,  $y_d$  is the desired output and  $*$  denotes the complex conjugate transpose. The terms  $R(j\omega)$  and  $Q(j\omega)$  are real-valued frequency dependant weightings that penalize the input ( $u$ ) and the tracking error ( $y -$

$y_d$ ) respectively. For a further discussion of trade-offs and various design approaches using this technique see (Brinkerhoff and Devasia, 1999).

By minimizing the cost function in Equation 7 the optimal input ( $u_{opt}$ ) is found as (Dewey et al., 1998)

$$u_{opt}(j\omega) = \left[ \frac{G^*(j\omega)Q(j\omega)}{R(j\omega) + G^*(j\omega)Q(j\omega)G(j\omega)} \right] \times x_d(j\omega), \quad (8)$$

where  $G(j\omega)$  is the transfer function of the piezopositioner system in the frequency domain.

## 3. EXPERIMENTS

The advantages of the integrated charge control and inverse feedforward approach are shown by applying the method to an experimental piezopositioner system. First, charge control is compared to voltage control (without inverse feedforward) to highlight the inherent hysteresis reduction capabilities of charge control. Second, inverse feedforward is compared to DC-gain control, where an input is found by dividing the desired trajectory ( $y_d$ ) by the DC gain of the system. This comparison is done using voltage control (not charge) to highlight the capabilities of the inverse feedforward method to reduce vibrations. Finally the two methods are integrated and compared to the previously mentioned cases. The experiments are run in open-loop to evaluate the effectiveness of the integrated method without additional control.

### 3.1 Experimental system

The piezopositioner used in these experiments was a 10cm long sectored piezoelectric-tube actuator made of lead zirconate titanate. The lateral position of the piezopositioner's tip was measured using a Kaman inductive sensor (SMU 9000-15N). For all experiments presented the desired trajectory ( $y_d$ ) was chosen as a filtered  $\pm 2\mu\text{m}$  triangular wave. Note that the filter was chosen such that only the first three components of the triangular waves' Fourier expansion were included.

### 3.2 Modeling the dynamics of the piezopositioner

To facilitate the use of inverse feedforward it is necessary to develop a mathematical model of the linear dynamics of the piezopositioner system. This was done by first measuring the linear vibrational dynamics of the charge and voltage controlled piezopositioners using a dynamic signal analyzer (DSA) (Stanford Research Systems SR785)

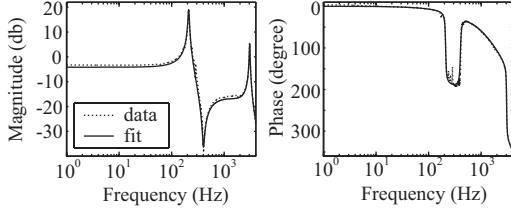


Fig. 2. Charge control frequency response plots for the experimental data (dotted line) and the transfer function fit (solid line)

and then developing transfer function models of the form

$$G_i(s) = k_i \frac{\prod_{m=1}^4 (s - z_{i,m})}{\prod_{n=1}^6 (s - p_{i,n})}, \quad (9)$$

where  $i$  denotes which control method was used (v for voltage control and c for charge control),  $k_i$  is the gain,  $z_{i,j}$  are the poles of the system and  $p_{i,j}$  are the zeros of the system. The gains for the two models were found to be  $k_v = 6.512 \times 10^6$  and  $k_c = 8.096 \times 10^6$ . The poles and zeros for the voltage and charge models are given in Tables 1 and 2 respectively.

Table 1. Voltage controlled piezopositioner model zeros and poles.

| m,n | zeros ( $z_{v,m}$ ) (rad/s) | poles ( $p_{v,n}$ )(rad/s) |
|-----|-----------------------------|----------------------------|
| 1   | $-82.77 + 2535.17j$         | $-32.06 + 1336.92j$        |
| 2   | $-82.77 - 2535.17j$         | $-32.06 - 1336.92j$        |
| 3   | $17376.26 + 33162.90j$      | $-9666.62$                 |
| 4   | $17376.26 - 33162.90j$      | $-309.54 + 19189.82j$      |
| 5   | -                           | $-309.54 - 19189.82j$      |
| 6   | -                           | $-30669.86$                |

Table 2. Charge controlled piezopositioner model zeros and poles.

| m,n | zeros ( $z_{c,m}$ ) (rad/s) | poles ( $p_{c,n}$ )(rad/s) |
|-----|-----------------------------|----------------------------|
| 1   | $-85.12 + 2530.93j$         | $-33.43 + 1325.75j$        |
| 2   | $-85.12 - 2530.93j$         | $-33.43 - 1325.75j$        |
| 3   | $19505.41 + 33323.36j$      | $-13533.10 + 3091.28j$     |
| 4   | $19505.41 - 33323.36j$      | $-13533.10 - 3091.28j$     |
| 5   | -                           | $-278.73 + 19190.57j$      |
| 6   | -                           | $-278.73 - 19190.57j$      |

The frequency response of the charge controlled transfer function model from Table 1 is compared to the experimental frequency response of the system obtained using the DSA in Figure 2. As seen in the Figures, the model adequately capture the system dynamics (similar agreement was found for the voltage controlled case and is thus not shown).

### 3.3 Results and discussion

To illustrate the advantages of the integrated charge-control/inverse-feedforward approach it is compared to the three other cases discussed earlier. Output trajectories for the 10Hz and 75Hz

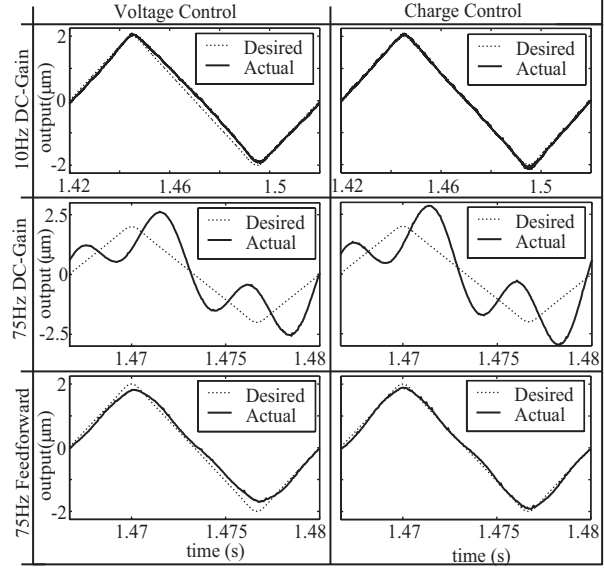


Fig. 3. Output trajectories for various methods. Actual output is shown as a solid line and desired output is shown as a dotted line.

cases are shown in Figure 3. The columns show different driving methods, while the rows show different control schemes. Root-Mean-Square (RMS) error ( $e_{rms}$ ) data for various operating frequencies ranging from 10Hz to 250Hz are presented in Table 3.

#### 3.3.1. Hysteresis reduction with charge control

Hysteresis is reduced using charge control, as can be seen in Figure 3 (row 1). The output from the voltage controlled piezopositioner (column 1) shows significant error (caused by hysteresis) when compared to the charge controlled output (column 2), which almost tracks the desired trajectory (dotted line) exactly. The amount of hysteresis reduction can be further seen by plotting the input versus output for both control methods as shown in Figure 4. Figure 4(a) shows the hysteresis loop for the voltage control case, while Figure 4(b) shows the loop for the charge control case. The amount of hysteresis reduction is quantified

Table 3. RMS error data ( $e_{rms}$ ) for the various methods, presented as a percentage of the operating range.

| f(Hz) | Voltage Control |        | Charge Control |        |
|-------|-----------------|--------|----------------|--------|
|       | DC (%)          | FF (%) | DC (%)         | FF (%) |
| 10    | 3.009           | 2.695  | 1.038          | 0.996  |
| 25    | 3.446           | 2.367  | 1.988          | 0.877  |
| 50    | 4.958           | 2.165  | 3.960          | 1.119  |
| 75    | 24.642          | 2.276  | 22.407         | 1.557  |
| 100   | 13.599          | 3.344  | 13.735         | 2.909  |
| 125   | 16.443          | 3.719  | 17.158         | 3.136  |
| 150   | 30.565          | 4.155  | 32.104         | 3.698  |
| 175   | 48.838          | 5.924  | 53.749         | 4.823  |
| 200   | 137.480         | 5.301  | 138.672        | 4.714  |
| 225   | 138.698         | 6.432  | 132.151        | 5.825  |
| 250   | 84.519          | 13.408 | 77.950         | 12.168 |

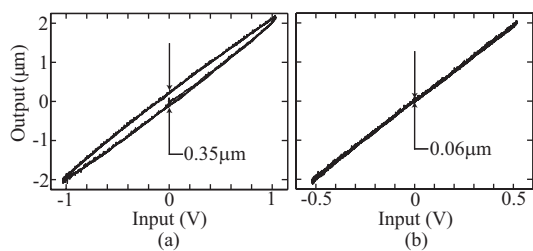


Fig. 4. Experimental hysteresis loops for a  $10Hz$  desired output of  $\pm 2\mu m$  using (a) voltage actuation and (b) charge actuation.

by determining the maximum output deviation at zero input (shown between the arrows). Using voltage control, the hysteresis is approximately  $0.35\mu m$  (8.8% of the range) compared to  $0.06\mu m$  (1.5%) when charge control is used, a reduction in hysteresis of approximately 83.0%. Thus, charge control reduces hysteresis.

Hysteresis is the dominant source of error at low frequencies (in this case  $10Hz - 50Hz$ ). As can be seen in Table 3, at low frequencies, for both the DC-gain and feedforward methods, the charge control case outperforms the voltage control case through the reduction of hysteresis (at some points providing greater than 60% reduction in error when compared to voltage control). As the frequency is increased it is more difficult to see hysteresis reduction (although it still occurs) because of the emergence of vibrations as the dominant source of error.

Charge control alone cannot reduce vibrational effects as can be seen in Figure 3 (row 2). To increase the effects of vibrations, the feedforward DC-gain input was sped up from  $10Hz$  to  $75Hz$ . Both voltage and charge control show significant vibration-caused error, thus charge (or voltage) control alone can not reduce vibrational effects.

**3.3.2. Induced mechanical vibration compensation using inverse feedforward** Induced mechanical vibrations can be reduced using the inverse feedforward method as can be seen in Figure 3 (rows 2 and 3, column 1). Using the voltage controlled piezopositioner model, given by Equation 9 and Table 1, and the optimal inverse feedforward method presented in section 2.2.1, a feedforward input was calculated to track the desired triangular trajectory. When this input was applied to the system the RMS error was reduced from 24.64% of the range using DC-gain control (row 2, column 1) to 2.28% (row 3) using inverse feedforward, a reduction in vibration-caused error of 88.7%.

Vibrational error tends to increase as the operating frequency approaches the first system resonance (in this case  $210Hz$ ), as seen in Table 3. The DC-Gain method does not take the vibrational

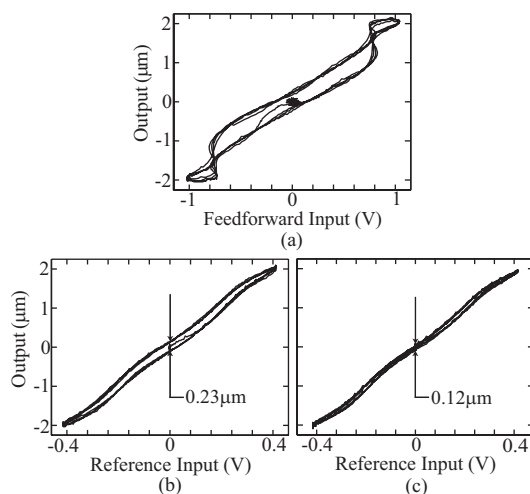


Fig. 5. Experimental hysteresis loops at  $75Hz$  for (a,b) voltage controlled feedforward, (c) charge controlled feedforward.

dynamics of the system into account, thus the error increases with frequency (column 2). However, when the feedforward method is applied (column 3) the error is reduced, most significantly as the operating frequency approaches the resonant peak.

The inverse feedforward method alone does not model the nonlinear hysteresis effect, and therefore cannot eliminate it without charge control. Therefore, significant hysteresis can be seen in the voltage controlled feedforward approach at  $75Hz$  (Figure 3, row 3, column 1). To further illustrate the amount of hysteresis present in the output, the feedforward input versus output plot for the  $75Hz$  case is shown in Figure 5(a). It is difficult to see hysteresis in this plot because the input necessary to reduce vibrations (plotted on the horizontal axes) contains vibration canceling oscillations. However, if instead the input to the inverse dynamics (the desired output ( $y_d$ )) is plotted versus the actual output, as shown in Figure 5(b), we can explicitly see the presence of hysteresis ( $0.23\mu m$  or 5.8% of the range). Note that vibrations still exist due to modeling errors. This shows that while the inverse feedforward method can compensate for vibrations, it cannot compensate for hysteresis.

**3.3.3. Integrated charge control and inverse feedforward** The integrated charge-control/inverse-feedforward approach can reduce both hysteresis- and vibration-caused errors, as seen in Figure 3 (row 3, column 2). The inverse feedforward input for the charge controlled piezopositioner was developed in the same manner as in the voltage controlled case. The hysteresis from the voltage controlled case (column 1) and the vibrations from DC-Gain case (row 2) have both been reduced (note that not all vibrations have been eliminated because of modeling errors). To quantify

the combined method's performance, RMS errors are compared. The combined method has an RMS error of 1.56% a 93.7% reduction when compared to the voltage controlled DC-Gain case and a reduction of 31.6% when compared to the voltage controlled feedforward case (column 1).

Charge control allows for hysteresis reduction at all frequencies even though it is difficult to see this effect in the presence of large vibrations. Once the vibrations are removed (using inverse feedforward), the reduction in hysteresis at 75Hz is more apparent and can be quantified using hysteresis loops as before. Therefore, the desired output is plotted versus actual output with charge control, as shown in Figure 5(c). The amount of hysteresis is reduced from 0.23 $\mu\text{m}$  (5.8% of the range) using voltage control to 0.12 $\mu\text{m}$  (3%) when charge control is used, a reduction of approximately 48.0%.

The advantages of the integrated approach at all frequencies can be seen in Table 3. The integrated charge control and inverse feedforward approach outperforms all other methods presented at all frequencies, showing that the integrated charge control and inverse feedforward approach can significantly reduce hysteresis and vibrations for a wide range of operating conditions.

#### 4. CONCLUSION

In this article we addressed the problems of hysteresis and induced mechanical vibrations in piezopositioners. Our main contribution was to integrate the use of charge control to reduce hysteresis and inverse feedforward to compensate for induced mechanical vibrations. This method was experimentally verified using a piezoelectric tube actuator and the advantages were shown by comparing its performance to other control methods. For example, at an operating frequency of 75Hz, the integrated approach could reduce error caused by hysteresis and vibrations by 93.7%.

#### REFERENCES

R. C. Barrett and C. F. Quate. Optical scan-correction system applied to atomic force microscopy. *Review of Scientific Instruments*, 62(6):1393–9, June 1991.

E. Bayo. A finite-element approach to control the end-point motion of a single link flexible robot. *Journal of Robotic Systems*, 4:63–74, 1987.

G. Binnig and D. P. E. Smith. Single-tube three-dimensional scanner for scanning tunneling microscopy. *Review of Scientific Instruments*, 57(8):1688–9, August 1986.

R. Brinkerhoff and S. Devasia. Output tracking for actuator deficient/redundant systems: multiple piezoactuator example. *Journal of*

*Guidance, Control, and Dynamics*, 23(2):370–3, 1999.

H. Cao and A. G. Evans. Nonlinear deformations of ferroelectric ceramics. *Journal of the American Ceramic Society*, 76:890–6, 1993.

D. Croft and S. Devasia. Hysteresis and vibration compensation for piezoactuators. *Journal of Guidance, Control, and Dynamics*, 21(5):710–17, Sep.-Oct. 1998.

D. Croft and S. Devasia. Vibration compensation for high speed scanning tunneling microscopy. *Review of Scientific Instruments*, December 1999.

J. S. Dewey, K. Leang, and S. Devasia. Experimental and theoretical results in output-trajectory redesign for flexible structures. *ASME Journal of Dynamic Systems, Measurement, and Control*, 120:456–61, December 1998.

A. J. Fleming and S. O. R. Moheimani. Sensorless vibration suppression and scan compensation for piezoelectric tube nanopositioners. *IEEE Transactions on Control Systems Technology*, 14(1):33–44, January 2006.

P. Ge and M. Jouaneh. Tracking control of a piezoceramic actuator. *IEEE Transaction on Control Systems Technology*, 4(3):209–16, 1996.

H. Hiura. Tailoring graphite layers by scanning tunneling microscopy. *Applied Surface Science*, 222:374–81, January 2003.

H. Kaizuka and B. Siu. A simple way to reduce hysteresis and creep when using piezoelectric actuators. *Japanese Journal of Applied Physics*, 27(5):L773–6, May 1988.

E. Kouno. A fast response piezoelectric actuator for servo correction of systematic errors in precision machining. *Annals of CIRP*, 33(1):369–72, 1982.

K. Kuhnene and H. Janocha. Inverse feedforward controller for complex hysteretic nonlinearities in smart-material systems. *Control and Intelligent Systems*, 29(3):74–83, 2001.

C. V. Newcomb and I. Flinn. Improving the linearity of piezoelectric ceramic actuators. *IEE Electronics Letters*, 18(11):442–3, May 1982.

Y. Okazaki. A micro-positioning tool post using a piezoelectric actuator for diamond tuning machines. *Precision Engineering*, 12(3):151–6, 1990.

C. F. Quate. Scanning probes as a lithography tool for nanostructures. *Surface Science*, 386:259–64, 1997.

G. Schitter and A. Stemmer. Model-based signal conditioning for high-speed atomic force and friction force microscopy. *Microelectronic Engineering*, 67-68:938–944, 2003.

K. A. Yi and R. J. Veillette. A charge controller for linear operation of a piezoelectric stack actuator. *IEEE Transactions on Control Systems Technology*, 13(4):517–26, July 2005.